Cell PRESS
Structure
Article

Structural Insights into the Mechanism of GTPase Activation in the GIMAP Family

David Schwefel,[1,2,7,*] B. Sivanandam Arasu,[1,2,6] Stephen F. Marino,[1,6] Björn Lamprecht,[1,3] Karl Köchert,[1] Eva Rosenbaum,[1] Jenny Eichhorst,[4] Burkhard Wiesner,[4] Joachim Behlke,[1] Oliver Rocks,[1] Stephan Mathas,[1,3] and Oliver Daumke[1,5,*]
[1]Max-Delbrück-Centrum für Molekulare Medizin, Robert-Rössle-Strasse 10, 13125 Berlin, Germany
[2]Institut für Chemie und Biochemie, Freie Universität Berlin, Takustrasse 3, 14195 Berlin, Germany
[3]Hematology, Oncology and Tumorimmunology, Charité-Universitätsmedizin Berlin, CVK, Augustenburger Platz 1, 13353 Berlin, Germany
[4]Leibniz-Institut für Molekulare Pharmakologie, Robert-Rössle-Str. 10, 13125 Berlin, Germany
[5]Institut für Medizinische Physik und Biophysik, Charité, Ziegelstrasse 5-9, 10117 Berlin, Germany
[6]These authors contributed equally to this work
[7]Present address: MRC National Institute for Medical Research, The Ridgeway, Mill Hill, London NW71AA, UK
*Correspondence: david.schwefel@nimr.mrc.ac.uk (D.S.), oliver.daumke@mdc-berlin.de (O.D.)
http://dx.doi.org/10.1016/j.str.2013.01.014

SUMMARY

GTPases of immunity-associated proteins (GIMAPs) are regulators of lymphocyte survival and homeostasis. We previously determined the structural basis of GTP-dependent GIMAP2 scaffold formation on lipid droplets. To understand how its GTP hydrolysis is activated, we screened for other GIMAPs on lipid droplets and identified GIMAP7. In contrast to GIMAP2, GIMAP7 displayed dimerization-stimulated GTP hydrolysis. The crystal structure of GTP-bound GIMAP7 showed a homodimer that assembled via the G domains, with the helical extensions protruding in opposite directions. We identified a catalytic arginine that is supplied to the opposing monomer to stimulate GTP hydrolysis. GIMAP7 also stimulated GTP hydrolysis by GIMAP2 via an analogous mechanism. Finally, we found *GIMAP2* and *GIMAP7* expression differentially regulated in several human T cell lymphoma lines. Our findings suggest that GTPase activity in the GIMAP family is controlled by homo- and heterodimerization. This may have implications for the differential roles of some GIMAPs in lymphocyte survival.

INTRODUCTION

GTPases of the immunity-associated proteins (GIMAPs) comprise a family of septin-related guanine nucleotide-binding (G) proteins which are present in vertebrates, plants and some viruses (reviewed in Nitta and Takahama, 2007). In vertebrates, *Gimap* genes are grouped in chromosomal clusters and are abundantly expressed in cells of the immune system (Poirier et al., 1999; Krücken et al., 2004). Animal models have demonstrated an essential role for GIMAPs in the development and maintenance of lymphocytes. The BioBreeding rat, with a frameshift mutation in *Gimap5*, as well as *Gimap5* knockout mice show a severe reduction in the number of peripheral T cells (MacMurray et al., 2002; Hornum et al., 2002; Michalkiewicz et al., 2004; Schulteis et al., 2008). BioBreeding rats develop autoimmune type 1 diabetes (T1D), whereas *Gimap5* knockout mice die 12–15 weeks after birth, likely due to immuno-inflammatory colitis (Barnes et al., 2010). Disturbed development and increased apoptosis rates are also observed in *Gimap5*-deficient hematopoietic stem and progenitor cells (Chen et al., 2011). Conditional knockout of *Gimap1* in mouse lymphoid tissues leads to a dramatic loss of peripheral T and B cells, extending the importance of the GIMAP family also to the B cell lineage (Saunders et al., 2010). In contrast, knockout of *Gimap4* in mice has no apparent effect on lymphocyte numbers (Schnell et al., 2006). Furthermore, lymphocytes isolated from *Gimap4* knockout mice or from a rat strain with reduced *Gimap4* expression show increased resistance to apoptotic stimuli, suggesting a pro-apoptotic function of GIMAP4 (Schnell et al., 2006; Carter et al., 2007). GIMAPs are also implicated in human diseases. Polymorphisms in the polyadenylation signal of *GIMAP5* were observed in patients with systemic lupus erythematosus (Hellquist et al., 2007). In regulatory T cells of patients with T1D, several *GIMAP* genes are downregulated compared to those of healthy individuals (Jailwala et al., 2009). Together with the finding that GIMAP3, GIMAP4, and GIMAP5 interact with pro- and anti-apoptotic members of the Bcl-2 family (Nitta et al., 2006; Chen et al., 2011), these data suggest that GIMAPs control the survival of lymphocytes by regulating apoptosis.

The seven human GIMAPs have molecular masses from 33 to 75 kDa. They are composed of an N-terminal G domain, followed by C-terminal extensions of 60–130 amino acids (Dion et al., 2005). As an exception, GIMAP8 consists of three such consecutive modules in one polypeptide. GIMAP1 and GIMAP5 each contain a single C-terminal transmembrane helix, which anchors them to the Golgi and the lysosomal compartments, respectively (Wong et al., 2010). Two C-terminal hydrophobic sequence stretches target human GIMAP2 to lipid droplets (Schwefel et al., 2010b). These hydrophobic sequences are not found in any mouse or rat GIMAP member.

Structural studies of GIMAP2 as a prototypic member of the membrane-anchored GIMAPs showed that the G domain has a canonical fold that phylogenetically relates them to the septin and dynamin GTPases (Schwefel et al., 2010b). GTP binding was proposed to induce assembly of GIMAP2 into a linear scaffold via two distinct interfaces, the G-interface across the

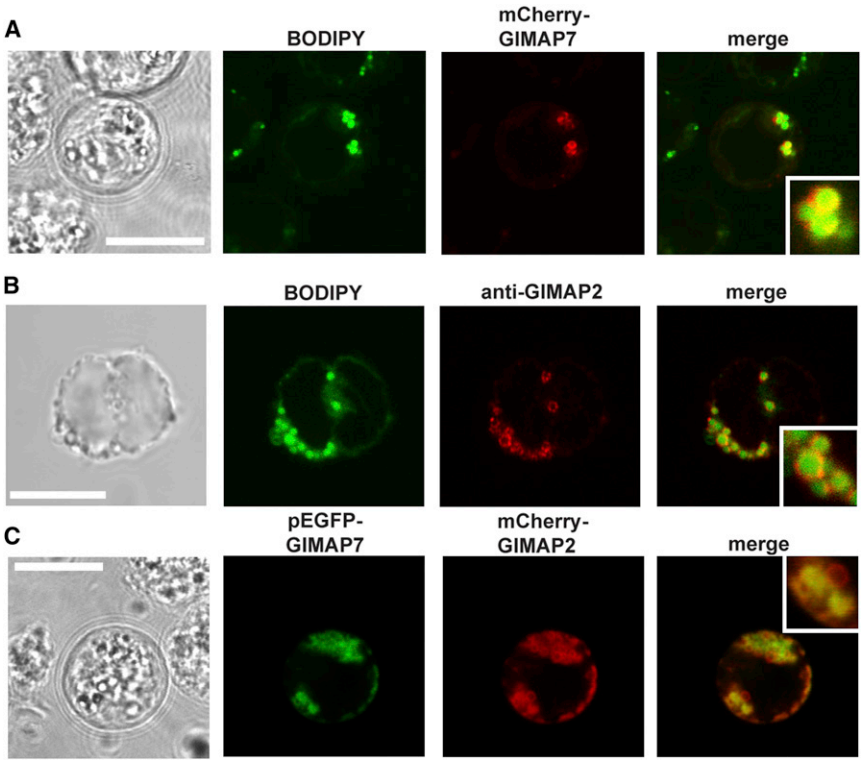

Figure 1. GIMAP2 and GIMAP7 Colocalize at the Surface of Lipid Droplets

(A) Localization of N-terminally mCherry-tagged GIMAP7 (red) in living Jurkat cells. Lipid droplets were costained with BODIPY 493/503 (green). All scale bars represent 10 μm.

(B) The localization of endogenous GIMAP2 (red) in Jurkat cells was determined by antibody staining and immunofluorescence analysis. Lipid droplets were costained with BODIPY 493/503 (green).

(C) N-terminally EGFP-tagged GIMAP7 (green) and N-terminally mCherry-tagged GIMAP2 (red) were coexpressed and visualized in living Jurkat cells.

See also Figure S1.

nucleotide-binding site and the C-interface at the backside of the G domain. The scaffold would be intrinsically stable because GIMAP2 was found not to hydrolyze GTP on its own.

In the present work, we followed up on our recent study to identify regulators of the GIMAP2 scaffold that can stimulate its GTPase activity and found GIMAP7 colocalizing with GIMAP2 on lipid droplets. We demonstrate that GIMAP7 can stimulate both its own GTPase activity and that of GIMAP2 by dimerization and the provision of a catalytic arginine finger. These findings may have important implications for understanding the molecular mechanisms by which GIMAPs regulate apoptosis.

RESULTS

GIMAP2 and GIMAP7 Colocalize on the Surface of Lipid Droplets

GIMAPs are related to the septin and dynamin GTPases (Schwefel et al., 2010b) that often show assembly-stimulated GTP hydrolysis (Gasper et al., 2009). We hypothesized that other GIMAP members might associate with GIMAP2 to activate its GTPase function. To probe for such partners, we conducted a subcellular localization screen for all human GIMAPs in the human Jurkat T cell leukemia cell line using N-terminal EGFP-GIMAP fusion proteins (Figure 1; Figure S1A available online). EGFP-GIMAP1 was found in a speckled pattern in the cytosol (Figure S1A), resembling the distribution of endogenous mouse GIMAP1 at the Golgi apparatus (Wong et al., 2010). No localization to lipid droplets was observed (Figure S1B). EGFP-GIMAP5 localized to intracellular vesicles of varying size (Figure S1A), in agreement with the previously described localization of endogenous mouse GIMAP5 to lysosomes (Wong et al., 2010). In approximately 10% of transfected cells, EGFP-GIMAP5 was additionally found at the plasma membrane (e.g., Figure S1A), but no localization to lipid droplets was observed (Figure S1B). EGFP-GIMAP4, EGFP-GIMAP6, and EGFP-GIMAP8 were distributed uniformly in the cytosol (Figure S1A). Strikingly, EGFP-GIMAP7 was found on the surface of spherical structures, resembling the staining obtained with EGFP-GIMAP2 (Figures 1A and S1A). We confirmed this localization to intracellular lipid droplets by costaining cells expressing mCherry-tagged GIMAP7 as well as endogenous GIMAP2 with the lipid droplet marker BODIPY 493/503 (Figures 1A and 1B). Upon coexpression of fluorescently-tagged GIMAP2 and GIMAP7, GIMAP7 fluorescence, while still localized to lipid droplets, was more diffuse, suggesting that GIMAP2 competes with GIMAP7 for common binding sites (Figure 1C).

Because GIMAP7 does not have a transmembrane anchor, we wondered whether it might be dynamically recruited to lipid droplets. We therefore analyzed the localization of mCherry-GIMAP7 in response to an apoptotic stimulus (anti-CD95, Figure S1C) or a stimulus inducing autophagy (suberoylanilide hydroxamic acid [SAHA]; Figure S1D). Neither of these stimuli markedly changed the localization of mCherry-GIMAP7. The lack of a specific antibody prevented us from determining the localization of endogenous GIMAP7 in Jurkat cells.

We previously showed that ectopic expression of GIMAP2 leads to a doubling of lipid droplet numbers (Schwefel et al., 2010b). In contrast, ectopic expression of GIMAP7 did not significantly influence lipid droplet numbers (Figure S1E).

GIMAP7 Shows Dimerization-Dependent GTP Hydrolysis

We then conducted a biochemical and structural analysis of GIMAP7. GIMAP7 was expressed as a GST-fusion in *Escherichia coli* and purified to homogeneity (Figures S2A and S2B). Because protein yields were low, we sought to improve the solubility of GIMAP7 by mutating a putative surface-exposed hydrophobic residue, Leu100, to glutamine (L100Q). Indeed, this resulted in a 10-fold increase in protein yields (Figure S2B). In the absence of nucleotide, this mutant was monomeric, as was

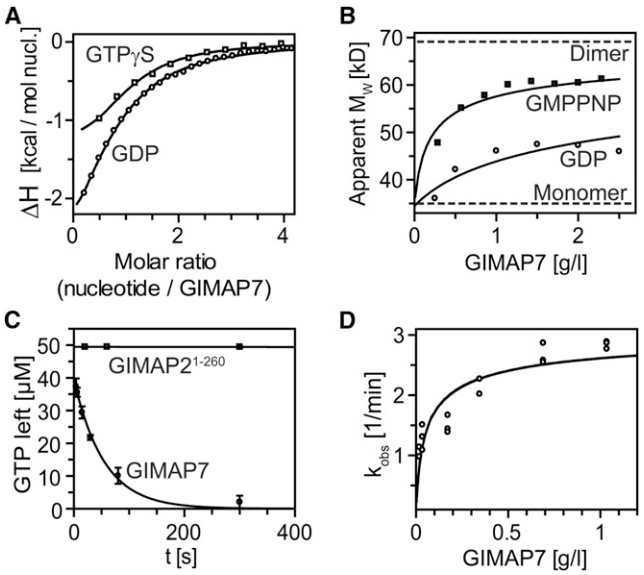

Figure 2. Biochemical Characterization of GIMAP7

(A) Nucleotide-binding affinities for GIMAP7 L100Q were determined using ITC. The following values were obtained from the fits: GIMAP7-GTP-γ-S (□): K_d = 10 ± 2 μM (n = 0.9), GIMAP7-GDP (○): K_d = 32 ± 2 μM (n = 0.8).

(B) Equilibrium sedimentation analytical ultracentrifugation experiments were performed to determine apparent molecular masses at the indicated GIMAP7 concentrations; 200 μM GMPPNP (■) or 500 μM GDP (○) were added to saturate GIMAP7 with the respective nucleotide. Monomer-dimer equilibria were fitted to the data obtained in the presence of GDP (K_d = 110 ± 20 μM) and GMPPNP (K_d = 9 ± 1 μM). Dashed lines indicate the molecular mass of the GIMAP7 monomer and dimer.

(C) Single turnover GTP hydrolysis reactions for GIMAP7 (■) were performed at 20°C, using a nucleotide and protein concentration of 50 μM. Plotted is the remaining GTP concentration versus time, determined as [GTP]/([GDP]+[GTP])×$[GTP]_{initial}$. Data points represent mean value ± SD of three independent experiments. An exponential decay was fitted to the data. For comparison, data of the cytosolic domain of GIMAP2 (residues 1–260, ■) are shown.

(D) Initial observed rates from multiple turnover GTP hydrolysis reactions in the presence of 500 μM GTP (○) were determined for GIMAP7 at the indicated protein concentrations (at least two independent measurements per data point). Data were fitted to a monomer-dimer equilibrium (Praefcke et al., 1999). A k_{max} value of 3.2 ± 0.2 min^{-1} and a K_d value of 1.2 ± 0.4 μM were obtained from the fit.

See also Figure S2.

Table 1. GIMAP7 Data Collection and Refinement Statistics

Protein	GIMAP7
Nucleotide	GMPPNP
Data collection	
Space group	P1
Cell dimensions	
a, b, c (Å)	45.9, 90.9, 114.7
α, β, γ (°)	77.3, 85.2, 89.2
Resolution (Å)	35–3.09 (3.28–3.09)[a]
R_{merge} (%)	10.9 (48.6)
I/σ (I)	7.24 (1.58)
Completeness (%)	95.3 (93.2)
Redundancy	1.8 (1.83)
Refinement	
Resolution (Å)	32.44–3.15
No. reflections	29758
R_{work}/R_{free}	23.4/30.5
No. atoms	
Protein	12423
Ligand/ion	198
Water	2
B-factors	
Protein	72.4
Ligand/ion	89.1
Water	52.5
Rmsds	
Bond lengths (Å)	0.004
Bond angles (°)	0.921

[a]Values in parentheses are for highest-resolution shell.

GIMAP7 wild-type, and also showed similar nucleotide hydrolysis properties (Figures S2C and S2D). Accordingly, all experiments requiring large amounts of purified protein, such as isothermal titration calorimetry (ITC) and crystallography, were carried out with the GIMAP7 L100Q mutant.

Nucleotide-binding affinities for GIMAP7 L100Q were determined by ITC. It bound the nonhydrolyzable GTP analog, guanosine 5′-O-[gamma-thio]triphosphate (GTP-γ-S), with an equilibrium dissociation constant (K_d) of 10 μM, and GDP with a K_d of 32 μM, in exothermic reactions (Figure 2A). These affinities are approximately 250-fold lower than the corresponding nucleotide affinities of GIMAP2. In analytical ultracentrifugation experiments, a monomer-dimer equilibrium with a K_d of 9 μM was observed in the presence of the nonhydrolyzable GTP analog guanosine 5′-[β,γ-imido]triphosphate (GMPPNP) (Figure 2B)—a 25-fold higher affinity for self-association than in the case of GIMAP2. GIMAP7 also dimerized in the presence of GDP, with a K_d of 100 μM (Figure 2B). In single turnover assays monitoring one cycle of GTP hydrolysis, GIMAP7 efficiently hydrolyzed GTP (Figure 2C). In multiple turnover assays (excess of GTP over protein), GIMAP7 showed a protein concentration-dependent increase in its specific GTPase activity with a k_{max} of 3.2 min^{-1} and an apparent K_d of 1.2 μM (Figure 2D), indicating that the GTPase reaction of GIMAP7 is stimulated by a cooperative mechanism.

Structure of GIMAP7

To obtain structural insights into catalysis, we crystallized GIMAP7 L100Q in the presence of GMPPNP. Crystals diffracted to a maximal resolution of 3.1 Å. The model was refined to an R_{work} of 23.4% and an R_{free} of 30.5% (Table 1; Figure S3A). The asymmetric unit of the crystals contained six copies of GIMAP7 (chains A–F); the best resolved chains, A and B, are described in the following. Clear electron density for the GMPPNP molecules was visible in the nucleotide-binding sites of all six GIMAP7 monomers (Figure S3B).

The N-terminal six residues of GIMAP7 were disordered. Residues 7–196 form a Ras-like G domain with the GIMAP-specific helix α3* inserted between strand β5 and helix α4 (Figures 3A and 3B). The overall structure of the G domains of GIMAP7

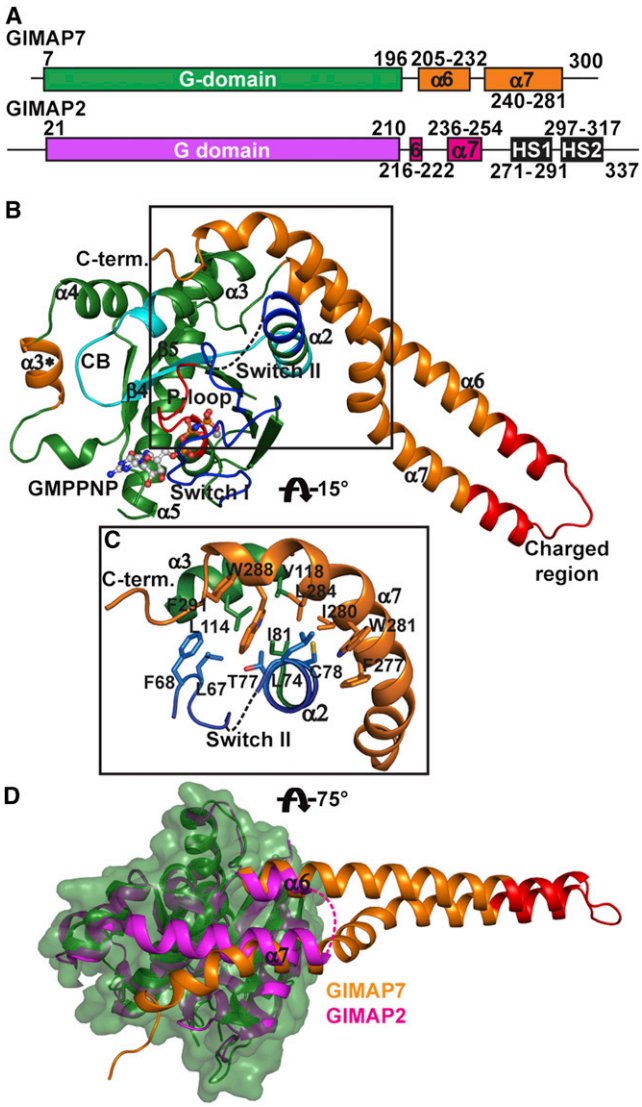

Figure 3. Structure of GIMAP7

(A) Schematic representation of the domain structure of GIMAP7 and GIMAP2 with amino acid positions indicated. HS, hydrophobic segment.

(B) Cartoon representation of the GMPPNP-bound GIMAP7 L100Q monomer. The G domain is shown in green, switch I and switch II in blue, the P loop in red, and the conserved box in cyan. Secondary structure elements differing from the core G domain of H-Ras (helix α3* and the C-terminal helices α6 and α7) are shown in orange. The nucleotide is shown in ball-and-stick representation.

(C) Detailed view of the C-terminal extension and its contact to switch II and the G domain. Selected residues are shown in stick representation.

(D) Comparison of the C-terminal extensions of GIMAP7 L100Q (orange) and GIMAP2 (magenta). The G domain of GIMAP7 is colored green and superimposed on the GIMAP2 G domain (magenta). The solvent-accessible surface of the GIMAP7 G domain is rendered semitransparent.

See also Figure S3.

and GIMAP2 can be superimposed with a root mean square deviation (rmsd) of 1.3 Å along 194 aligned residues. The most notable difference was observed in the partially disordered switch II region, where Gly66 of GIMAP7 is stabilized by a backbone interaction with the GMPPNP γ-phosphate, in contrast to the corresponding Asp80 of GIMAP2, which is displaced by the γ-phosphate of GTP (Figure S3C). We previously suggested a function of switch II in GIMAP2 in regulating the release of helix α7 from the G domain. The divergent architectures might indicate a different function of switch II in GIMAP7.

In the absence of stabilizing crystal contacts, the C-terminal extension is partially disordered in five of the six GIMAP7 monomers in the asymmetric unit (Figure S4A). In chain A, however, it folds into two elongated helices, α6 and α7 (Figure 3B). Half of the amino acids in this 90 residue helical domain are charged and project toward the solvent. A multiple sequence alignment shows that the closely related GIMAP4 has a similar charged sequence stretch in this region (Figure S3A). The C-terminal end of helix α7 folds against a hydrophobic patch of the G domain created by the switch II region and helix α3 (Figure 3C).

A superposition of the G domains of GIMAP7 and GIMAP2 allowed for a direct comparison of their C-terminal extensions (Figure 3D). Helix α6 and α7 in GIMAP7 are greatly extended in length compared to those in GIMAP2. The short helix α6 from GIMAP2 is equivalent to the beginning of helix α6 in GIMAP7. The flexible linker between α6 and α7 in GIMAP2 is replaced by the extended helical region of GIMAP7. The C-terminal end of helix α7 in GIMAP7 projects along the G domain with a tilt of approximately 25° compared to the corresponding region of GIMAP2. Helix α6 and α7 in GIMAP7 also form a larger interface with the G domain compared to GIMAP2 (1100 Å^2 compared to 840 Å^2). These differences suggest that the C-terminal extension of GIMAP7 is more tightly associated to its G domain than that in GIMAP2 and probably remains attached during the GTPase cycle, in contrast to the proposed displacement of α7 in GIMAP2 upon GTP binding (Schwefel et al., 2010b).

Structure of the Catalytically Active GIMAP7 Dimer

The six GIMAP7 monomers in the crystal structure were arranged in three almost identical dimers (rmsd = 0.6–0.8 Å for 450–500 aligned residues per dimer; Figures 4A, 4B, and S4A). Analogous to GIMAP2, switch I was stabilized by a contact of Thr44 with the γ-phosphate of the nucleotide. In turn, residues in switch I (e.g., Ile38, Ala40) contacted helix α3* of the opposing monomer, explaining the GTP-dependence of dimerization (Figures 4C and S3A). Conserved box residue Glu106, along with the adjacent Lys110, form a symmetric double salt bridge across the dimer interface; additionally, Gln100, introduced by the L100Q mutation, forms a double hydrogen bond with the symmetry-related amino acid of the opposing molecule (Figure S4B). As in GIMAP2, Glu135 in the G4 motif binds to the guanine base in cis, whereas the following Glu136 contacts the guanine base of the opposing molecule in trans (Figure 4C).

The GIMAP7 dimer interface is composed of the conserved box, switch I, the G4 loop and helix α3* (Figures 4B and 4C). It shows a much larger buried surface area of 1500 Å^2 as compared to the 600 Å^2 of the corresponding GIMAP2 dimer. This is in line with the lower equilibrium dissociation constant of the GIMAP7 dimer determined in solution (Figure 2B). However, the principle assembly mode of GIMAPs via the G-interface appears to be conserved.

The conserved box residue Arg117 in GIMAP2 is crucial for dimerization by forming a hydrogen bond to Gln114 (Schwefel

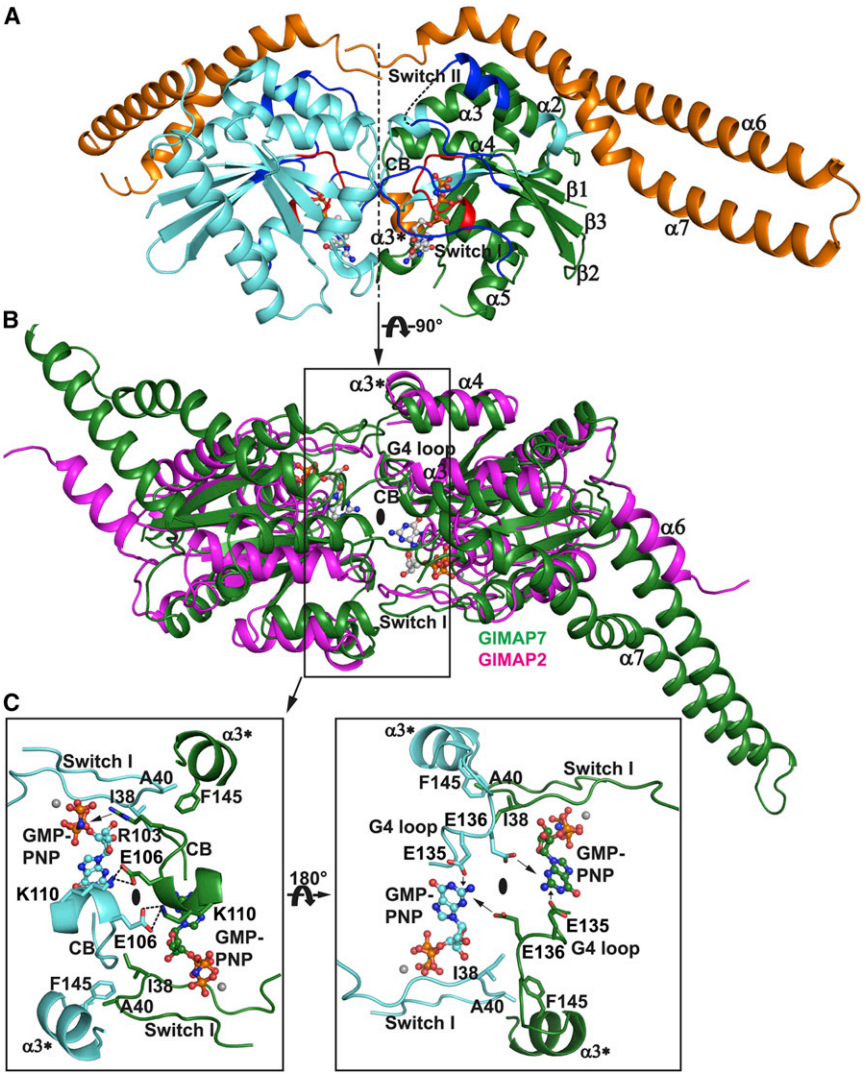

Figure 4. The G-Interface Dimer of GIMAP7

(A) Cartoon representation of the GIMAP7 L100Q dimer, with one protomer shown in the same colors as in Figure 3B and the other protomer shown in cyan/orange. The pseudo 2-fold dimer axis is indicated by a dashed line.

(B) Superposition of the GIMAP7 L100Q (green) and GIMAP2 (magenta, Protein Data Bank code 2XTN) G-domain dimers. The pseudo 2-fold dimer axis is indicated by an ellipse.

(C) Detailed view of the GIMAP7 dimer interface. To the right, a 180° rotation is shown. Selected residues are shown in stick representation.

See also Figure S4.

et al., 2010b). The corresponding Arg103 in GIMAP7 is disordered in five of the six GIMAP7 chains within the asymmetric unit. Only in chain B is interpretable electron density for Arg103 apparent, showing that the residue forms water-mediated hydrogen bonds to the nitrogen between the β- and γ-phosphate of GMPPNP in the opposing protomer (Figure 5A). In this orientation, the arginine would be ideally situated to act as a catalytic residue in the opposing molecule by counteracting the developing negative charge during GTP hydrolysis.

To characterize the catalytic mechanism of GIMAP7, mutagenesis studies were performed (Figures 5B–5D). Glu136 in the center of the G-interface was mutated to the more bulky tryptophan to interfere with dimerization. The E136W mutation did not affect the binding affinity for GTP-γ-S, as determined by ITC measurement, but it did, surprisingly, result in an endothermic binding reaction (Figure 5B). Indeed, it reduced GTP-promoted dimerization (Figure 5C) and almost completely abolished the GTPase reaction (Figure 5D), indicating that dimerization via the G-interface is required for the stimulated GTPase activity.

A mutation of the proposed catalytic residue, Arg103, to aspartate also did not interfere with the affinity for GTP-γ-S (Figure 5B). In contrast to the E136W mutation, the R103D mutation did not influence GTP-dependent dimerization (Figure 5C). This is in agreement with the observation that Arg103 is mostly disordered in the GIMAP7 homodimers and apparently not involved in dimerization. The mutation did, however, completely block the GTPase activity (Figure 5D). These features are hallmarks of a catalytic residue and indicate that Arg103 in GIMAP7 acts as a catalytic arginine finger in trans that is inserted into the catalytic machinery of the opposing molecule during the GTPase reaction.

GIMAP7 Stimulates GTP Hydrolysis of GIMAP2

Considering our colocalization results, we next asked whether GIMAP7 also stimulates the GTPase reaction of GIMAP2 via a similar mechanism involving heterodimerization. As previously reported, the cytosolic domain of GIMAP2 (residues 1–260, used in all experiments below) on its own displayed no GTPase activity (Schwefel et al., 2010b). However, addition of 5 μM GIMAP7 to 50 μM GIMAP2 using single turnover conditions for GIMAP2 increased overall GTP hydrolysis in this mixture 2.6-fold as compared to the GTPase reaction of 5 μM GIMAP7 alone (Figure 6A). This effect was not due to protein crowding because addition of a 10-fold molar excess of GST to GIMAP7 did not influence its hydrolytic activity.

To further investigate this effect, we performed a GTP protection assay using alkaline phosphatase. This enzyme readily hydrolyzes GTP in solution to guanine, whereas it cannot hydrolyze nucleotides that are bound and therefore protected from hydrolysis by a protein (John et al., 1990). In agreement with the high affinity for GTP (K_d = 40 nM; Schwefel et al., 2010b), GIMAP2 protected more than 40% of GTP from hydrolysis by alkaline phosphatase over a period of 30 min, indicating that GIMAP2 releases bound GTP very slowly (Figure 6A). This is consistent with our observation that GIMAP2 expressed in

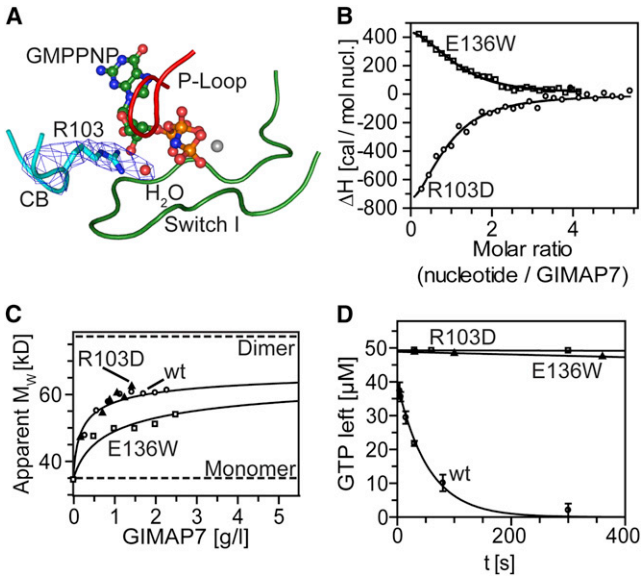

Figure 5. Dimerization-Dependent GTPase Activity of GIMAP7 Employs a Catalytic Arginine Finger

(A) $2F_O$-F_C density, contoured at 1 σ, is shown for Arg103 in chain B and the water molecule connecting the arginine side chain with the opposing GMPPNP molecule via hydrogen bonding. Chain A is shown in green and chain B in cyan; the P loop of chain A is colored in red. The magnesium ion is shown as a gray sphere.

(B) Nucleotide-binding affinities of GIMAP7 mutants to GTP-γ-S were determined using ITC, as in Figure 2A. The following values were obtained from the fits: R103D (○), K_d = 14 ± 4 μM (n = 0.8); E136W (□), K_d = 19 ± 3 μM (n = 1.1).

(C) Sedimentation equilibrium ultracentrifugation experiments for GIMAP7 R103D (▲) and E136W (□) in the presence of 200 μM GMPPNP, as in Figure 2B. The following values for a monomer-dimer equilibrium were obtained from the data fits: GIMAP7 E136W: K_d = 47 ± 6 μM, GIMAP7 R103D: K_d = 8 ± 1 μM. Data for GIMAP7 (○, Figure 2B) in the presence of 200 μM GMPPNP are shown for comparison.

(D) Nucleotide hydrolysis of the E136W (▲) and R103D (□) mutants of GIMAP7 were measured by HPLC in a single turnover assay (using a protein and nucleotide concentration of 50 μM), as in Figure 2C. GTP hydrolysis of GIMAP7 (○, Figure 2C) is shown for comparison. Data points are mean values ± SD of three independent experiments.

bacteria retains GTP during the purification process (Schwefel et al., 2010b). However, when GIMAP2 was combined with 5 μM GIMAP7, almost all of the GTP in the reaction mixture was hydrolyzed within 30 min (Figure 6A). This suggests that GIMAP7 can indeed stimulate GTP hydrolysis in GIMAP2.

The enhanced GTPase rate in GIMAP2/GIMAP7 mixtures was further characterized using single site mutations in the G-interface of both proteins. The GIMAP2 S54A mutation in switch I prevents homodimerization (Schwefel et al., 2010b) and abrogated the increased GTPase rate in the GIMAP2-GIMAP7 mixture (Figure 6B), suggesting that stabilization of switch I in GIMAP2 is also important for heterodimer formation. The GIMAP2 R117D mutant, which cannot homodimerize (Schwefel et al., 2010b), also did not show enhanced GTPase rates in our assay (Figure 6B).

As shown in Figures 5C and 5D, the E136W mutation in GIMAP7 impaired homodimerization and almost completely eliminated the GTPase activity. Remarkably, when this mutant was incubated with GIMAP2, efficient GTP hydrolysis was observed (Figure 6B). This strongly supports the existence of a GIMAP2-GIMAP7 heterodimer whose architecture appears to differ in detail from that of the GIMAP7 homodimer. The rate enhancement effect was critically dependent on the presence of the catalytic Arg103 in GIMAP7, since a mixture of GIMAP7 R103D and GIMAP2 showed no GTPase activity at all.

To further characterize the reaction, multiple turnover assays (excess of GTP) were performed. Increasing concentrations of GIMAP2 were titrated against a constant concentration (2.5 μM) of GIMAP7 (Figure 6C). In these assays, the reaction rate increased with increasing GIMAP2 concentration. The concentration of GIMAP2 for half-maximal activation of overall GTP hydrolysis was approximately 7 μM, which is in the range of the homo-dimerization affinity of GIMAP7. This suggests a low affinity interaction between GIMAP2 and GIMAP7. Addition of increasing concentrations of the GIMAP2 R117D mutant to GIMAP7 did not substantially affect the GTPase rate seen with GIMAP7 alone (Figure 6C). Only very marginal GTPase activity was observed for the GIMAP7 R103D mutant in the presence of 50 μM GIMAP2, implying that GIMAP2 does not supply its Arg117 as catalytic residue to complement the active site of GIMAP7 (Figure 6D).

Taken together, our data point to a mechanism where GIMAP2 and GIMAP7 heterodimerize with low affinity in a transient manner, and GIMAP7 acts as GTPase-activating protein for GIMAP2 by supplying its catalytic arginine finger in trans.

Expression of *GIMAP*s in Anaplastic Large Cell Lymphoma Cell Lines

GIMAP1, GIMAP4, and GIMAP5 are implicated in the regulation of lymphocyte survival (Nitta et al., 2006; Schnell et al., 2006; Schulteis et al., 2008; Barnes et al., 2010; Saunders et al., 2010). Furthermore, GIMAPs have been identified as target genes of NOTCH signaling (Chadwick et al., 2009; Wang et al., 2011), a key pathway for malignant transformation of T lymphoid cells. We therefore screened a panel of human T-cell leukemia (Jurkat, KE-37, Molt-14, H9) and anaplastic large cell lymphoma (ALCL) cell lines for alterations of *GIMAP* expression by semi-quantitative reverse transcriptase (RT)-PCR analyses (Figure 7). As a control, we included purified $CD3^+$ and $CD4^+$ T cells from the peripheral blood of healthy donors. In the purified normal $CD3^+$ and $CD4^+$ T cells, mRNA expression of all seven *GIMAP* family members was detectable. Apart from a few exceptions (e.g., *GIMAP8* in KE-37 cells or *GIMAP4* in Molt-14 cells), all *GIMAP*s were expressed in the T cell leukemia-derived cell lines investigated. In contrast, mRNA expression of various *GIMAP*s was strongly reduced or even lost in most of the ALCL-derived lymphoma cell lines (Figure 7). Interestingly, whereas *GIMAP2* mRNA was still present in all examined ALCL cell lines, expression of *GIMAP7* and the closely related *GIMAP4* was uniformly lost.

DISCUSSION

G proteins cycle between an active GTP-bound state and an inactive GDP-bound state, and these states can be interconverted by nucleotide exchange or GTP hydrolysis (reviewed in Vetter and Wittinghofer, 2001). In G proteins of the Ras superfamily, GTP hydrolysis is stimulated by association with

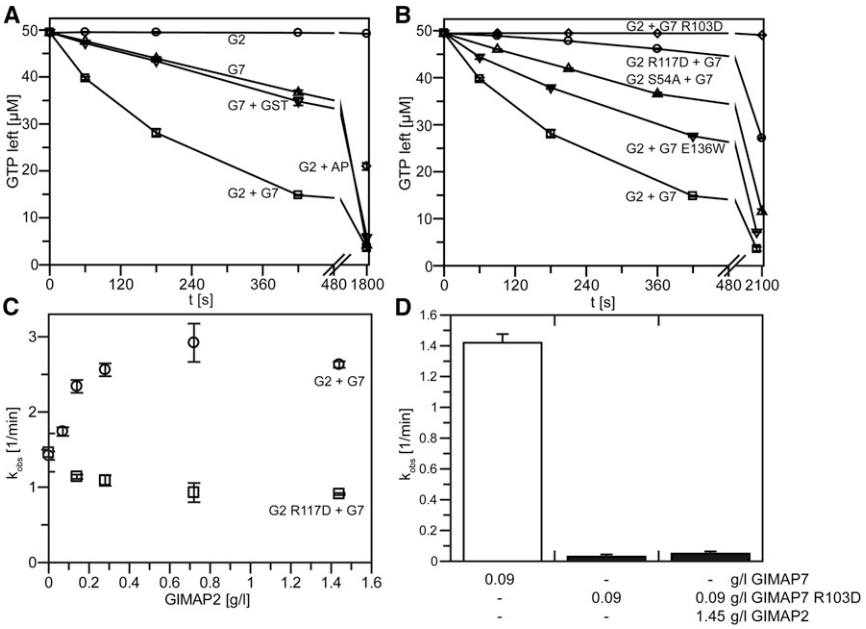

Figure 6. GTPase Enhancement in Mixtures of GIMAP2 and GIMAP7

(A) Nucleotide hydrolysis was measured by HPLC, as in Figure 2C, employing 50 μM GIMAP2 (○), 5 μM GIMAP7 (△), and a mixture of 50 μM GIMAP2 together with 5 μM GIMAP7 (□) at a GTP concentration of 50 μM (complete nucleotide loading of GIMAP2). Further control experiments were conducted using mixtures of 50 μM GST and 5 μM GIMAP7 (▽) as well as 50 μM GIMAP2 and 0.2 U alkaline phosphatase (◇, AP). This amount of AP hydrolyzes 50 μM free GTP in less than a minute (data not shown). Data points are mean values ± SD of three independent experiments. Note that under these conditions, GIMAP7 is not fully saturated with nucleotide, resulting in a lower GTPase rate than in multiple turnover assays.

(B) Mutational analysis of the GTPase rate enhancement under single turnover conditions for GIMAP2. Mixtures of 50 μM GIMAP2 and 5 μM GIMAP7 R103D (◇), 50 μM GIMAP2, and 5 μM GIMAP7 E136W (▽), 50 μM GIMAP2 R117D, and 5 μM GIMAP7 (○) as well as 50 μM GIMAP2 S54A and 5 μM GIMAP7 (△) were analyzed for their GTPase activities. The hydrolysis reaction for 50 μM GIMAP2 together with 5 μM GIMAP7 (□) is shown for comparison (see Figure 6A). Data points are mean values ± SD of three independent experiments.

(C) Analysis of the GTPase rate enhancement of GIMAP2/GIMAP2 R117D and GIMAP7 using multiple turnover conditions (500 μM GTP). A constant GIMAP7 concentration of 2.5 μM and increasing concentrations of GIMAP2 (○) or GIMAP2 R117D (□) were used. Rates were calculated by normalizing the reaction velocity to the GIMAP7 concentration. Data points represent mean values ± range of two independent experiments.

(D) The GIMAP7 R103D mutant at a concentration of 2.5 μM is catalytically inactive and can be stimulated only to a minor extent by 50 μM GIMAP2. For comparison, the GTPase activity of 2.5 μM GIMAP7 is shown (see Figure 6C). Data points represent mean values ± range of two independent experiments.

GTPase-activating proteins (GAPs) which often supply a catalytic arginine residue in trans to complement the active site (Bos et al., 2007). In a second class of G proteins, GTPase activity is triggered by nucleotide-dependent dimerization of the G domains (Gasper et al., 2009). These G proteins include members of the dynamin superfamily (Praefcke and McMahon, 2004), septins (Sirajuddin et al., 2007), and the septin-related Toc proteins (Sun et al., 2002; Koenig et al., 2008). Dimerization in dynamins induces rearrangements of catalytic residues in cis, thereby inducing GTPase stimulation (e.g., Ghosh et al., 2006). In septins, a threonine residue in switch I is stabilized upon dimerization and positions the catalytic water molecule in cis for GTPase activation (Sirajuddin et al., 2009). For Toc proteins, a conserved arginine is in the vicinity of the nucleotide-binding cleft of the opposing molecule, but its role in catalysis is disputed (Sun et al., 2002; Koenig et al., 2008). Our results indicate that GIMAPs also belong to the group of G proteins whose GTPase activity is stimulated by dimerization. We show that a highly conserved arginine from the conserved box motif in the GIMAP G-interface has a dual function. In the GIMAP2 homodimer, it stabilizes the dimerization interface as a mere structural residue. In this way, further scaffold assembly via a second dimerization interface may proceed (Schwefel et al., 2010b). By contrast, we demonstrate here that the equivalent arginine residue in GIMAP7 acts as a catalytic arginine finger in the GIMAP7 homodimer and GIMAP7-GIMAP2 heterodimer, by complementing the active site of the opposing monomer. Thus, the conserved box arginine serves a dual function by promoting self-association and stimulating GTP hydrolysis. The observed colocalization of GIMAP2 and GIMAP7 at lipid droplets and our biochemical data demonstrating the specific ability of GIMAP7 to stimulate GTP hydrolysis in GIMAP2 argue for a functional interplay of these two GTPases in vivo.

Also in other GTPase families, interactions between members of two functionally distinct subgroups have been shown to modulate catalytic activity, for example in the immunity-related GTPases (IRG) (Hunn et al., 2008). In contrast to our findings, members of one IRG subgroup assemble with proteins of the second subgroup to prevent GTP loading and activation. The proposed catalytic mechanism, however, involves homodimerization (Pawlowski et al., 2011). Heterodimer formation and subsequent GTPase activation is also observed in the signal recognition particle (SRP) and its receptor (SRPR) (reviewed in Grudnik et al., 2009). However, compared to the septin and dynamin GTPases, the SRP-SRPR system appears to have evolved independently (Schwefel et al., 2010b).

Taking into account the known biochemical and functional characteristics of individual GIMAP family members, a pattern emerges. GIMAP1, GIMAP2, and GIMAP5 appear to be stably associated with specific cellular compartments by their C-terminal hydrophobic sequences. GIMAP2 (Schwefel et al., 2010b) and GIMAP5 (D.S. and O.D., unpublished data) bind GTP with high affinity but cannot hydrolyze it on their own. Their high local concentration at membrane surfaces and their restricted mobility due to the C-terminal membrane anchors might promote the formation of a GIMAP scaffold in the GTP-bound form, despite their low dimerization affinity (Schwefel and Daumke, 2011; Wu et al., 2011). In the GDP-bound

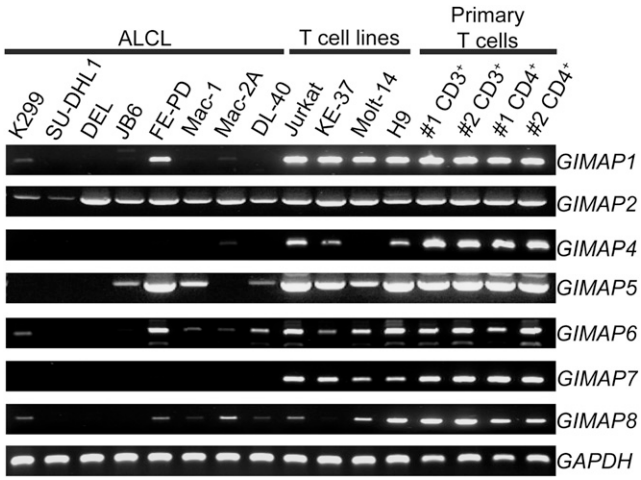

Figure 7. Altered Expression of Human *GIMAP*s in ALCL-Derived Lymphoma Cell Lines

mRNA expression of the seven human *GIMAP* family members was determined by semiquantitative RT-PCR in purified $CD3^+$ and $CD4^+$ T cells from the peripheral blood of two healthy donors (#1, #2; primary T cells), a panel of T cell leukemia cell lines (T cell lines) and a panel of eight ALCL-derived lymphoma cell lines (ALCL). mRNA expression of *GAPDH* was analyzed as a control.

form, these GIMAP scaffolds were proposed to disassemble (Schwefel et al., 2010b).

In contrast, GIMAP7 binds guanine nucleotides with lower affinity and catalyzes GTP hydrolysis by a dimerization-dependent mechanism. Similarly, GTPase activity has been demonstrated for the closely related GIMAP4 (Cambot et al., 2002). Based on the results for GIMAP2 and GIMAP7, we propose a scenario in which catalytically active GIMAP members stimulate GTP hydrolysis in the catalytically inactive GIMAPs. Such a model could, for example, rationalize the proposed opposing functions of GIMAP4 and GIMAP5 in lymphocyte survival observed in animal models (e.g., Chen et al., 2011; Schnell et al., 2006). In its GTP-bound form, a GIMAP5 scaffold can form and may inhibit apoptosis. GIMAP4 may disrupt these scaffolds by heterodimerization with and stimulation of GTPase activity in GIMAP5. Such a model is also consistent with our *GIMAP* mRNA expression data in lymphoma cell lines, which largely agrees with mRNA microarray analyses from primary ALCL (Eckerle et al., 2009). *GIMAP4* and *GIMAP7* are completely downregulated in ALCL cell lines compared to different T cell lines, whereas *GIMAP2* is present in the whole ALCL panel and *GIMAP5* in half of the ALCL lines.

In summary, our study provides the structural and biochemical framework for examining the differential functions of GIMAPs in lymphocyte survival, for elucidating the molecular details of GIMAP interactions with their target proteins, and for identifying the cellular pathways involving GIMAPs that might be altered in human T cell lymphoma.

EXPERIMENTAL PROCEDURES

Protein Expression and Purification

GIMAP2 and its mutants were expressed and purified as described (Schwefel et al., 2010a). GIMAP7 and mutants were expressed and purified in the same way, with an additional wash step during affinity chromatography using 50 mM HEPES pH 7.5, 500 mM NaCl, 2.5 mM DTT, 2 mM $MgCl_2$, 0.1 mM GDP, and 1% CHAPS. Protein at a concentration of about 30 mg/ml was flash-frozen in small aliquots in liquid nitrogen and stored at −80°C. All GTPase experiments within one figure panel were carried out with one batch of protein, due to slight variations in the GTPase activity of different preparations and loss of activity after extended storage (>24 hr) at 4°C.

Crystallization and Data Collection

GMPPNP (Jena Bioscience) and $MgCl_2$ were added to a final concentration of 2 mM. Crystallization trials were performed using the hanging-drop vapor-diffusion method at 20°C. One microliter of the protein solution at a GIMAP7 concentration of 10 mg/ml was mixed with an equal volume of reservoir solution containing 19% PEG 3350 and 100 mM MOPS, pH 6.5. Crystal plates with dimensions of 0.2 mm × 0.2 mm × 0.01 mm appeared after 1 day. Single plates were separated and transferred to a cryosolution containing 10 mM HEPES pH 7.5, 300 mM NaCl, 2.5 mM DTT, 2 mM $MgCl_2$, 2 mM GMPPNP, 32% PEG 3350, 100 mM MOPS pH 6.5, and flash-cooled in liquid nitrogen. A data set was collected on beamline 14.1 at BESSY and processed using the XDS program suite (Kabsch, 1993).

Structure Analysis and Refinement

The structure of GIMAP7 was solved by molecular replacement using Molrep (Vagin and Teplyakov, 1997) with GTP-bound $GIMAP2^{1–234}$ as a search model (Protein Data Base code 2XTN). Model building and refinement were carried out using the programs Coot (Emsley and Cowtan, 2004) and Phenix (Murshudov et al., 1997). The final model of GIMAP7 contains six protein molecules in the asymmetric unit encompassing residues 8–69, 73–170, 173–295 of chain A; 7–227, 258–293 of chain B; 8–230, 263–293 of chain C; 9–51, 57–169, 173–193, 198–216, 273–299 of chain D; 7–236, 242–297 of chain E; and 8–68, 73–138, 141–227, 250–262, 266–291 of chain F. Of all residues, 97.4% are in the favored region of the Ramachandran plot and 0.33% are outliers. All protein structure representations were prepared using PyMOL (DeLano,W.L. The PyMol Molecular Graphics System. DeLano Scientific, Palo Alto, CA, USA; http://www.pymol.org). Solvent-accessible interface areas in each monomer buried during dimer formation were calculated using the PISA server (Krissinel and Henrick, 2007). Rmsd values were calculated using Coot.

Isothermal Titration Calorimetry

ITC experiments were performed on a VP-ITC (GE Healthcare, München, Germany) at 8°C using a protein concentration of 50 μM and a nucleotide concentration of 1 mM. Dissociation constants were calculated using the vendor-supplied Origin software.

Sedimentation Equilibrium Analytical Ultracentrifugation

Molecular mass studies of GIMAP7 constructs in 10 mM HEPES pH 7.5, 150 mM NaCl, 2 mM $MgCl_2$, 2.5 mM DTT and the indicated nucleotide concentrations were performed in an XL-A type analytical ultracentrifuge (Beckman). Experiments were carried out using six-channel cells with 12 mm optical path length and the capacity to handle three solvent-solution pairs of about 70 μl volume. Sedimentation equilibrium was reached after 2 hr of overspeed at 24,000 rpm followed by an equilibrium speed of 20,000 rpm for about 30 hr at 10°C. The radial absorbance in each compartment was recorded at three different wavelengths between 270 and 290 nm depending on the concentration used in the experiments. Molecular mass determinations employed the global fit of the three radial distributions using the programs POLYMOLE or POLYMOLA (Behlke et al., 1997). Assuming a monomer-dimer equilibrium, the molecular mass, M, can be treated approximately as a weight average parameter (M_w). This value is a composite of the monomer molecular mass (M_m) and that of the dimer (M_d) and the partial concentrations of monomers, c_m, and dimers, c_d.

$$M_w = \frac{(c_m \times M_m + c_d \times M_d)}{c_m + c_d}.$$

Therefore, the equilibrium constant, K_d, can be determined by

$$K_d = \frac{c_m^2}{c_d}.$$

GTP Hydrolysis Assays

Single turnover GTPase rates at the indicated protein concentrations were determined in 20 mM HEPES pH 7.5, 150 mM NaCl, 2.5 mM DTT, 5 mM KCl, and 5 mM $MgCl_2$ at 20°C in the presence of 50 μM GTP using standard HPLC detection. In short, 20 μl reactions were applied to a Ti-Series 1050 HPLC system (Hewlett-Packard), equipped with a reversed-phase ODS-2 Hypersil column (Thermo Scientific). The running buffer contained 10 mM Tetra-n-butylammonium bromide, 100 mM potassium phosphate (pH 6.5), and 7.5% acetonitrile. Denatured proteins were adsorbed on a Nucleosil 100 C18 guard column (Knauer), and separated nucleotides were detected by measuring the absorption at 254 nm.

For multiple turnover assays, a saturating GTP concentration of 500 μM was used. Rates derived from a linear fit to the initial reaction rates (<40% GTP hydrolyzed) were plotted against the protein concentrations. For determination of the apparent K_d and k_{max}, a simple binding model was fitted to the data that describes the interaction of two GTP-bound GIMAP7 molecules inducing GTP hydrolysis (Praefcke et al., 1999).

Cell Culture

Human ALCL cell lines (t[2;5]-positive: K299, SU-DHL-1, DEL, JB6; t[2;5]-negative: FE-PD, Mac-1, Mac-2A, DL-40) and T cell leukemia-derived cell lines (Jurkat, KE-37, Molt-14 and H9) were cultured as described (Mathas et al., 2006). $CD3^+$ and $CD4^+$ peripheral T cells were purified from blood of healthy donors using CD3 or CD4 MicroBeads (Miltenyi Biotec, Germany). The purity of $CD3^+$ and $CD4^+$ T cells was greater than 97%, as determined by staining of purified cells with a PE-conjugated anti-CD3 (Dako Deutschland GmbH) or anti-CD4 antibody (BD Biosciences) and subsequent fluorescence-activated cell sorter (FACS) analysis using a FACSCalibur flow cytometer (Becton Dickinson, Germany). The use of the human material was approved by the Local Ethical Committee of the Charité, Medical University Berlin, and performed in accordance with the Declaration of Helsinki.

RNA Preparation and RT-PCR Analysis

Total RNA was prepared using the RNeasy kit (QIAGEN). For RT-PCR analyses, first-strand cDNA synthesis was performed by use of the first-strand cDNA synthesis kit (Roche, Germany) adding oligo-p(dT)15 primer according to the manufacturer's recommendation. See Supplemental Experimental Procedures for primer sequences. All PCR products were verified by sequencing.

Microscopy

For live cell microscopy, 5×10^6 cells were washed with PBS, centrifuged at 1,500 g for 5 min, and resuspended in 0.5 ml OPTIMEM medium (Invitrogen). Cells were electroporated with 30 μg of plasmid DNA coding for mCherry or EGFP fused N-terminally to the indicated construct in a BioRad Gene Pulser (exponential protocol, V = 300 V, C = 500 μF). Forty-eight hours later, cells were washed with PBS and stained with BODIPY 493/503 according to (Gocze and Freeman, 1994). After two more washing steps with PBS, cells were resuspended in 25 μl RPMI medium, and live cells were imaged using Zeiss LSM 510 or Olympus FV1000 confocal microscopes (BODIPY: λ_{exc} = 488 nm, λ_{em} = BP505–530). Immunofluorescence procedures can be found in the Supplemental Experimental Procedures.

ACCESSION NUMBERS

The Protein Data Bank accession number for the atomic coordinates and structure factors reported in this paper is 3ZJC.

SUPPLEMENTAL INFORMATION

Supplemental Information includes four figures and Supplemental Experimental Procedures and can be found with this article online at http://dx.doi.org/10.1016/j.str.2013.01.014.

ACKNOWLEDGMENTS

We would like to thank D. Rüthnick for help during protein preparation and crystallization, S. Werner and M. Papst for technical assistance, and the BESSY II staff at BL14.1, especially U. Müller, for help with data collection. We also would like to thank K. Fälber and M. Krauß for valuable discussions on the manuscript. This project was supported by a grant from the German Research Foundation (SFB958/A12), by a Career Development Award of The International Human Frontier Science Program Organization, and by an EMBO Young Investigator Fellowship to O.D.

Received: July 12, 2012
Revised: January 17, 2013
Accepted: January 19, 2013
Published: February 28, 2013

REFERENCES

Barnes, M.J., Aksoylar, H., Krebs, P., Bourdeau, T., Arnold, C.N., Xia, Y., Khovananth, K., Engel, I., Sovath, S., Lampe, K., et al. (2010). Loss of T cell and B cell quiescence precedes the onset of microbial flora-dependent wasting disease and intestinal inflammation in Gimap5-deficient mice. J. Immunol. *184*, 3743–3754.

Behlke, J., Ristau, O., and Schönfeld, H.J. (1997). Nucleotide-dependent complex formation between the Escherichia coli chaperonins GroEL and GroES studied under equilibrium conditions. Biochemistry *36*, 5149–5156.

Bos, J.L., Rehmann, H., and Wittinghofer, A. (2007). GEFs and GAPs: critical elements in the control of small G proteins. Cell *129*, 865–877.

Cambot, M., Aresta, S., Kahn-Perlès, B., de Gunzburg, J., and Roméo, P.H. (2002). Human immune associated nucleotide 1: a member of a new guanosine triphosphatase family expressed in resting T and B cells. Blood *99*, 3293–3301.

Carter, C., Dion, C., Schnell, S., Coadwell, W.J., Graham, M., Hepburn, L., Morgan, G., Hutchings, A., Pascall, J.C., Jacobs, H., et al. (2007). A natural hypomorphic variant of the apoptosis regulator Gimap4/IAN1. J. Immunol. *179*, 1784–1795.

Chadwick, N., Zeef, L., Portillo, V., Fennessy, C., Warrander, F., Hoyle, S., and Buckle, A.M. (2009). Identification of novel Notch target genes in T cell leukaemia. Mol. Cancer *8*, 35.

Chen, Y., Yu, M., Dai, X., Zogg, M., Wen, R., Weiler, H., and Wang, D. (2011). Critical role for Gimap5 in the survival of mouse hematopoietic stem and progenitor cells. J. Exp. Med. *208*, 923–935.

Dion, C., Carter, C., Hepburn, L., Coadwell, W.J., Morgan, G., Graham, M., Pugh, N., Anderson, G., Butcher, G.W., and Miller, J.R. (2005). Expression of the Ian family of putative GTPases during T cell development and description of an Ian with three sets of GTP/GDP-binding motifs. Int. Immunol. *17*, 1257–1268.

Eckerle, S., Brune, V., Döring, C., Tiacci, E., Bohle, V., Sundström, C., Kodet, R., Paulli, M., Falini, B., Klapper, W., et al. (2009). Gene expression profiling of isolated tumour cells from anaplastic large cell lymphomas: insights into its cellular origin, pathogenesis and relation to Hodgkin lymphoma. Leukemia *23*, 2129–2138.

Emsley, P., and Cowtan, K. (2004). Coot: model-building tools for molecular graphics. Acta Crystallogr. D Biol. Crystallogr. *60*, 2126–2132.

Gasper, R., Meyer, S., Gotthardt, K., Sirajuddin, M., and Wittinghofer, A. (2009). It takes two to tango: regulation of G proteins by dimerization. Nat. Rev. Mol. Cell Biol. *10*, 423–429.

Ghosh, A., Praefcke, G.J., Renault, L., Wittinghofer, A., and Herrmann, C. (2006). How guanylate-binding proteins achieve assembly-stimulated processive cleavage of GTP to GMP. Nature *440*, 101–104.

Gocze, P.M., and Freeman, D.A. (1994). Factors underlying the variability of lipid droplet fluorescence in MA-10 Leydig tumor cells. Cytometry *17*, 151–158.

Grudnik, P., Bange, G., and Sinning, I. (2009). Protein targeting by the signal recognition particle. Biol. Chem. *390*, 775–782.

Hellquist, A., Zucchelli, M., Kivinen, K., Saarialho-Kere, U., Koskenmies, S., Widen, E., Julkunen, H., Wong, A., Karjalainen-Lindsberg, M.L., Skoog, T., et al. (2007). The human GIMAP5 gene has a common polyadenylation

polymorphism increasing risk to systemic lupus erythematosus. J. Med. Genet. *44*, 314–321.

Hornum, L., Rømer, J., and Markholst, H. (2002). The diabetes-prone BB rat carries a frameshift mutation in Ian4, a positional candidate of Iddm1. Diabetes *51*, 1972–1979.

Hunn, J.P., Koenen-Waisman, S., Papic, N., Schroeder, N., Pawlowski, N., Lange, R., Kaiser, F., Zerrahn, J., Martens, S., and Howard, J.C. (2008). Regulatory interactions between IRG resistance GTPases in the cellular response to Toxoplasma gondii. EMBO J. *27*, 2495–2509.

Jailwala, P., Waukau, J., Glisic, S., Jana, S., Ehlenbach, S., Hessner, M., Alemzadeh, R., Matsuyama, S., Laud, P., Wang, X., and Ghosh, S. (2009). Apoptosis of CD4+ CD25(high) T cells in type 1 diabetes may be partially mediated by IL-2 deprivation. PLoS ONE *4*, e6527.

John, J., Sohmen, R., Feuerstein, J., Linke, R., Wittinghofer, A., and Goody, R.S. (1990). Kinetics of interaction of nucleotides with nucleotide-free H-ras p21. Biochemistry *29*, 6058–6065.

Kabsch, W. (1993). Automatic processing of rotation diffraction data from crystals of initially unknown symmetry and cell constants. J. Appl. Cryst. *26*, 795–800.

Koenig, P., Oreb, M., Höfle, A., Kaltofen, S., Rippe, K., Sinning, I., Schleiff, E., and Tews, I. (2008). The GTPase cycle of the chloroplast import receptors Toc33/Toc34: implications from monomeric and dimeric structures. Structure *16*, 585–596.

Krissinel, E., and Henrick, K. (2007). Inference of macromolecular assemblies from crystalline state. J. Mol. Biol. *372*, 774–797.

Krücken, J., Schroetel, R.M., Müller, I.U., Saïdani, N., Marinovski, P., Benten, W.P., Stamm, O., and Wunderlich, F. (2004). Comparative analysis of the human gimap gene cluster encoding a novel GTPase family. Gene *341*, 291–304.

MacMurray, A.J., Moralejo, D.H., Kwitek, A.E., Rutledge, E.A., Van Yserloo, B., Gohlke, P., Speros, S.J., Snyder, B., Schaefer, J., Bieg, S., et al. (2002). Lymphopenia in the BB rat model of type 1 diabetes is due to a mutation in a novel immune-associated nucleotide (Ian)-related gene. Genome Res. *12*, 1029–1039.

Mathas, S., Janz, M., Hummel, F., Hummel, M., Wollert-Wulf, B., Lusatis, S., Anagnostopoulos, I., Lietz, A., Sigvardsson, M., Jundt, F., et al. (2006). Intrinsic inhibition of transcription factor E2A by HLH proteins ABF-1 and Id2 mediates reprogramming of neoplastic B cells in Hodgkin lymphoma. Nat. Immunol. *7*, 207–215.

Michalkiewicz, M., Michalkiewicz, T., Ettinger, R.A., Rutledge, E.A., Fuller, J.M., Moralejo, D.H., Van Yserloo, B., MacMurray, A.J., Kwitek, A.E., Jacob, H.J., et al. (2004). Transgenic rescue demonstrates involvement of the Ian5 gene in T cell development in the rat. Physiol. Genomics *19*, 228–232.

Murshudov, G.N., Vagin, A.A., and Dodson, E.J. (1997). Refinement of macromolecular structures by the maximum-likelihood method. Acta Crystallogr. D Biol. Crystallogr. *53*, 240–255.

Nitta, T., and Takahama, Y. (2007). The lymphocyte guard-IANs: regulation of lymphocyte survival by IAN/GIMAP family proteins. Trends Immunol. *28*, 58–65.

Nitta, T., Nasreen, M., Seike, T., Goji, A., Ohigashi, I., Miyazaki, T., Ohta, T., Kanno, M., and Takahama, Y. (2006). IAN family critically regulates survival and development of T lymphocytes. PLoS Biol. *4*, e103.

Pawlowski, N., Khaminets, A., Hunn, J.P., Papic, N., Schmidt, A., Uthaiah, R.C., Lange, R., Vopper, G., Martens, S., Wolf, E., and Howard, J.C. (2011). The activation mechanism of Irga6, an interferon-inducible GTPase contributing to mouse resistance against Toxoplasma gondii. BMC Biol. *9*, 7.

Poirier, G.M., Anderson, G., Huvar, A., Wagaman, P.C., Shuttleworth, J., Jenkinson, E., Jackson, M.R., Peterson, P.A., and Erlander, M.G. (1999). Immune-associated nucleotide-1 (IAN-1) is a thymic selection marker and defines a novel gene family conserved in plants. J. Immunol. *163*, 4960–4969.

Praefcke, G.J., and McMahon, H.T. (2004). The dynamin superfamily: universal membrane tubulation and fission molecules? Nat. Rev. Mol. Cell Biol. *5*, 133–147.

Praefcke, G.J., Geyer, M., Schwemmle, M., Robert Kalbitzer, H., and Herrmann, C. (1999). Nucleotide-binding characteristics of human guanylate-binding protein 1 (hGBP1) and identification of the third GTP-binding motif. J. Mol. Biol. *292*, 321–332.

Saunders, A., Webb, L.M., Janas, M.L., Hutchings, A., Pascall, J., Carter, C., Pugh, N., Morgan, G., Turner, M., and Butcher, G.W. (2010). Putative GTPase GIMAP1 is critical for the development of mature B and T lymphocytes. Blood *115*, 3249–3257.

Schnell, S., Démollière, C., van den Berk, P., and Jacobs, H. (2006). Gimap4 accelerates T-cell death. Blood *108*, 591–599.

Schulteis, R.D., Chu, H., Dai, X., Chen, Y., Edwards, B., Haribhai, D., Williams, C.B., Malarkannan, S., Hessner, M.J., Glisic-Milosavljevic, S., et al. (2008). Impaired survival of peripheral T cells, disrupted NK/NKT cell development, and liver failure in mice lacking Gimap5. Blood *112*, 4905–4914.

Schwefel, D., and Daumke, O. (2011). GTP-dependent scaffold formation in the GTPase of Immunity Associated Protein family. Small GTPases *2*, 27–30.

Schwefel, D., Fröhlich, C., and Daumke, O. (2010a). Purification, crystallization and preliminary X-ray analysis of human GIMAP2. Acta Crystallogr. Sect. F Struct. Biol. Cryst. Commun. *66*, 725–729.

Schwefel, D., Fröhlich, C., Eichhorst, J., Wiesner, B., Behlke, J., Aravind, L., and Daumke, O. (2010b). Structural basis of oligomerization in septin-like GTPase of immunity-associated protein 2 (GIMAP2). Proc. Natl. Acad. Sci. USA *107*, 20299–20304.

Sirajuddin, M., Farkasovsky, M., Hauer, F., Kühlmann, D., Macara, I.G., Weyand, M., Stark, H., and Wittinghofer, A. (2007). Structural insight into filament formation by mammalian septins. Nature *449*, 311–315.

Sirajuddin, M., Farkasovsky, M., Zent, E., and Wittinghofer, A. (2009). GTP-induced conformational changes in septins and implications for function. Proc. Natl. Acad. Sci. USA *106*, 16592–16597.

Sun, Y.J., Forouhar, F., Li Hm, H.M., Tu, S.L., Yeh, Y.H., Kao, S., Shr, H.L., Chou, C.C., Chen, C., and Hsiao, C.D. (2002). Crystal structure of pea Toc34, a novel GTPase of the chloroplast protein translocon. Nat. Struct. Biol. *9*, 95–100.

Vagin, A., and Teplyakov, A. (1997). MOLREP: an automated program for molecular replacement. J. Appl. Cryst. *30*, 1022–1025.

Vetter, I.R., and Wittinghofer, A. (2001). The guanine nucleotide-binding switch in three dimensions. Science *294*, 1299–1304.

Wang, H., Zou, J., Zhao, B., Johannsen, E., Ashworth, T., Wong, H., Pear, W.S., Schug, J., Blacklow, S.C., Arnett, K.L., et al. (2011). Genome-wide analysis reveals conserved and divergent features of Notch1/RBPJ binding in human and murine T-lymphoblastic leukemia cells. Proc. Natl. Acad. Sci. USA *108*, 14908–14913.

Wong, V.W., Saunders, A.E., Hutchings, A., Pascall, J.C., Carter, C., Bright, N.A., Walker, S.A., Ktistakis, N.T., and Butcher, G.W. (2010). The autoimmunity-related GIMAP5 GTPase is a lysosome-associated protein. Self Nonself *1*, 259–268.

Wu, Y., Vendome, J., Shapiro, L., Ben-Shaul, A., and Honig, B. (2011). Transforming binding affinities from three dimensions to two with application to cadherin clustering. Nature *475*, 510–513.